

Enhancing micro-perforated panel attenuation by partitioning the adjoining cavity

J. Liu, D.W. Herrin *

Department of Mechanical Engineering, College of Engineering, University of Kentucky, 151 RGAN Building, Lexington, KY 40506-0503, United States

ARTICLE INFO

Article history:

Received 30 April 2009

Received in revised form 20 July 2009

Accepted 27 July 2009

Available online 15 September 2009

Keywords:

Micro-perforated panel

Air cavity partitioning

Sound attenuation

ABSTRACT

The sound attenuation performance of micro-perforated panels (MPP) with adjoining air cavity is investigated for a plenum. The sound field inside of a plenum is compared for two cases. In the first case, the plenum is treated with an MPP and adjoining air cavity without any partitioning. For the second case, the adjoining air cavity is partitioned into a number of sub-cavities. The resulting sound pressure fields indicate that partitioning the adjoining air cavity increases the overall sound attenuation due to the MPP by approximately 4 dB. The explanation for this phenomenon was investigated by measuring the sound pressure level on planes in front of the MPP. Additionally, boundary element analyses were conducted to simulate the effect of the MPP and adjoining cavity with and without partitioning on the sound field in the plenum. It was demonstrated that a MPP can be modeled as a transfer impedance and that partitioning the adjoining cavity enhances attenuation to acoustic modes that propagate transverse to the MPP.

© 2009 Elsevier Ltd. All rights reserved.

1. Introduction

Micro-perforated panel (MPP) absorbers are attractive because they provide effective sound absorption in environments where fibrous or porous materials deteriorate. For ordinary perforated panels, pore diameters are on the order of millimeters or even centimeters with modest inherent acoustic resistance. Conversely, MPP absorbers are a relatively new development in which pore diameters are sub-millimeter size ranging from 1 mm to as small as 0.1 mm. Because of the small pores, MPP absorbers provide acoustic resistance enabling improved sound attenuation. Compared to traditional sound absorbing materials, MPP absorbers are unique because they are non-combustible, high temperature and wear resistant, fiber free and aesthetically pleasing. Due to these benefits, MPP absorbers are being increasingly used in automotive, aerospace, and building applications [1,2].

Another benefit of MPP absorbers is that they can be easily tuned to provide a broadband sound absorption especially at low frequencies. According to Maa's theory [3–5], four design parameters control the impedance of MPP absorbers. These parameters including pore diameter d , panel porosity σ , thickness t , and cavity depth D are illustrated in Fig. 1. Maa expressed the impedance (z) as

$$z = \frac{\Delta p}{u} = \frac{32\eta t}{\sigma \rho c d^2} \left(\left(1 + \frac{\beta^2}{32} \right)^{1/2} + \frac{\sqrt{2}}{8} \beta \frac{d}{t} \right) + j \left(\frac{\omega t}{\sigma c} \left(1 + \left(3^2 + \frac{\beta^2}{2} \right)^{-1/2} + 0.85 \frac{d}{t} \right) - \cot \frac{\omega D}{c} \right) \quad (1)$$

where ω is the frequency, c is the speed of sound, and β is a perforate constant dependent on the properties of the fluid. β is given as

$$\beta = d \sqrt{\omega \rho / 4\eta} \quad (2)$$

where η is the viscosity and ρ is the mass density of air.

Based on Eq. (1), a theoretical parameter study can be conducted to investigate the impact of each of these four parameters on the absorption coefficient [1,6]. For instance, varying the pore diameter affects the bandwidth of the sound absorption. Most importantly, MPP absorbers can be tuned by varying the cavity depth in effect determining the frequency range where the MPP absorber is most effective. The MPP will have maximum absorption when the depth of the cavity is approximately one-quarter wavelength. This occurs when the acoustic particle velocity is highest in the pore. Varying porosity, pore diameter, and thickness minimally change the frequency where the maximum frequency occurs [1,6].

It is noteworthy that Maa's theory assumes normal incidence. However, MPP absorbers have been applied in cases where the incidence is grazing or diffuse. In the case of HVAC (heating,

* Corresponding author.

E-mail address: dherrin@engr.uky.edu (D.W. Herrin).

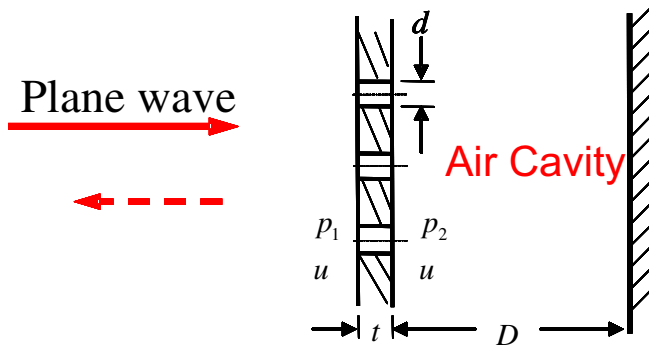


Fig. 1. Schematic of MPP and adjoining air cavity.

ventilation and air conditioning) systems, MPP absorbers are being used along the sides of straight duct, in elbows and also in plena [1,7,8]. Grazing and normal incidence can be assumed in the case of straight ducts and elbows respectively at low frequencies. If installed in plena, both grazing and normal incidence can be expected at low frequencies. However, diffuse incidence occurs at high frequencies in HVAC systems.

2. Adding partitioning to back cavity

In prior work by the authors [6], an experimental study was undertaken to determine the insertion loss due to an MPP absorber in a silencer. This insertion loss was compared to that of open cell foam occupying the same volume in the silencer. The result showed that the overall insertion loss of the MPP absorber is approximately 3 dB lower than that of the foam.

In order to improve the MPP performance, various strategies to treat the air cavity have been proposed and examined [9–11]. These include partitioning the air cavity, arranging absorbers in parallel while varying cavity depths, layering absorbers, and introducing a thin fabric to the back of the MPP. Yairi et al. [9] concluded that partitioning the air cavity was especially effective. The authors' prior results agreed with what Yairi et al. observed [6]. In particular, it was found that partitioning the cavity improved the overall insertion loss by 2 dB resulting in MPP performance roughly comparable to foam.

The effect of partitioning the air cavity has been noticed by several researchers. Toyoda and Takahashi investigated the effect of subdividing the adjoining air cavity on the oblique incident transmission loss of an MPP [12]. Their results suggested that partitioning the air cavity improved the transmission loss at mid-frequencies by means of providing a motion-constraint condition to the particles so that the acoustic wave could only propagate normal to the MPP. Yairi et al. tested the MPP's with an alternative honeycomb partitioning in the adjoining cavity. Agreeing with Toyoda and Takahashi, they showed that the honeycomb affected only the oblique incidence absorption coefficient and had a minimal effect on normal incidence absorption [9].

Hillereau et al. [13] considered a more complicated case where honeycomb cell walls themselves were also porous. They studied the sound attenuation of an ordinary perforated panel under grazing incidence. They concluded that the variation of the honeycomb porosity had a significant impact on the acoustic attenuation of a given perforated facing panel. In this situation, the partitioning cannot be simplified as a device that merely forces the oblique incident wave into a normal incident wave in the cell.

The purpose of this paper is to experimentally investigate the effect of partitioning the adjoining air cavity on plenum acoustics. Refs. [9] and [12] investigated the physics of an MPP with adjoining

cavity for different incident wave angles. The current work builds on this by looking at the effect of the MPP and adjoining cavity on the plenum cavity (the cavity of interest). Like Refs. [9] and [12] the partitioning behind the MPP is non-porous though it is light and not rigid.

3. Experimental configuration

The objective of this work was to better understand acoustic behavior inside a plenum with and without honeycomb partitioning. Fenech et al. [14] conducted a similar study where the effect of a MPP on the acoustic modes inside of a closed cavity was investigated. They noted that the MPP was effective at damping the acoustic cavity modes normal to the MPP but ineffective at damping modes tangential to the MPP. This paper examines the significance of partitioning the adjoining cavity on the acoustic modes in a plenum. For this investigation, a loudspeaker was attached via a short tube to a plenum having dimensions $0.96 \text{ m} \times 0.57 \text{ m} \times 0.42 \text{ m}$. Fig. 2 shows an end view of the silencer with the honeycomb partitioning of the air cavity. The experimental setup is shown in Fig. 3.

The MPP utilized was a micro-slit absorber (MSA) which shares many characteristics with an MPP. The perforation shape of an MSA is an irregular slit instead of circular hole. Maa [15] found that a MSA is virtually identical to an MPP except that an MSA has slightly smaller resistance and larger reactance. Rather than predicting the impedance using Maa's theory, the transfer impedance was measured in an impedance tube using a similar technique to the two-cavity method proposed by Wu et al. [16]. The measured transfer impedance is shown in Fig. 4. Fig. 5 compares the normal incident absorption coefficient of an MPP with 65 mm cavity predicted using the transfer impedance with that measured directly using the two-microphone method [17].

The MPP treatment was placed on the side of the plenum opposite the source. Several different configurations were applied and tested. These included three cases:

- Untreated (i.e. no MPP absorber or partitioning installed).
- MPP absorber with 65 mm back cavity and no partitioning.
- MPP absorber with 65 mm back cavity with a cardboard partitioning. Cells are honeycomb shaped. If the partitioning is placed in the plenum without an MPP facing, a small effect was noted [6].

For each condition, sound pressure was measured at a plane located 95 mm from the treated end of the plenum (30 mm anterior

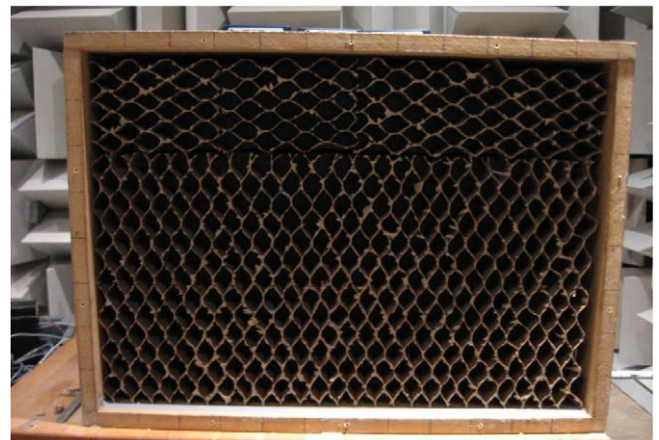


Fig. 2. Photograph showing cardboard partitioning in the cavity behind the MPP.

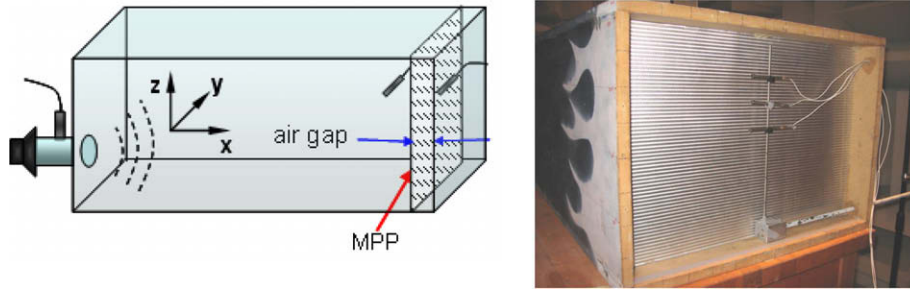


Fig. 3. Schematic (on left) and photograph (on right) showing measurement setup.

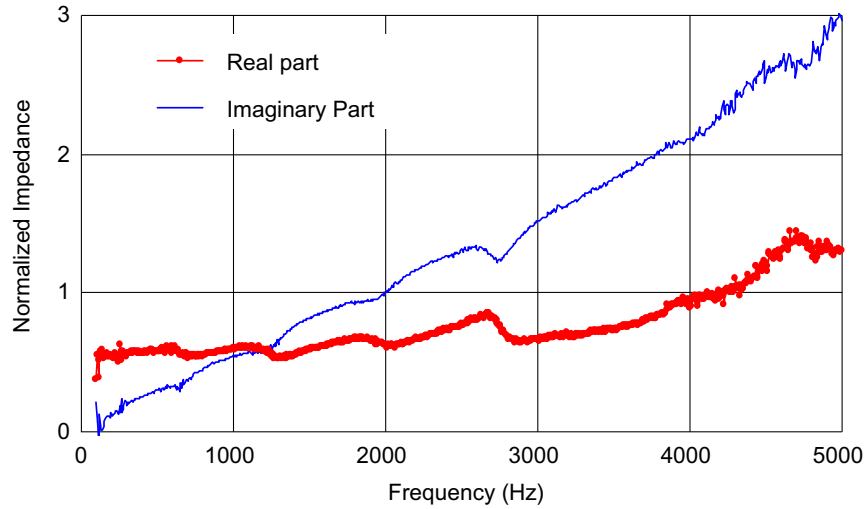


Fig. 4. Measured transfer impedance of an aluminum micro-slit absorber.

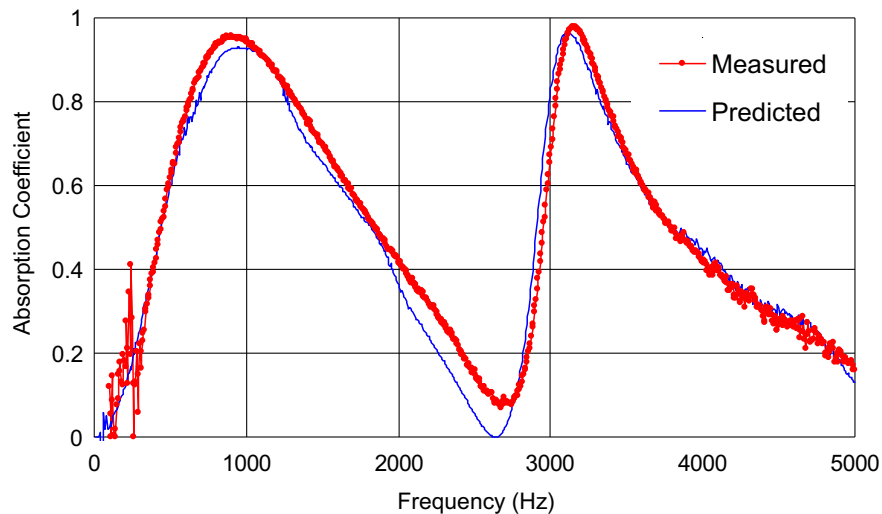


Fig. 5. Normal incident absorption coefficient of MPP with 65 mm air cavity.

to the MPP with a 65 mm adjoining cavity depth). In each case, the measurement plane consisted of 54 points. Measurement points were spaced 3.8 cm and 5.6 cm apart in horizontal and vertical directions respectively.

The natural frequencies of the plenum can be calculated using.

$$f(l, m, n) = \frac{c}{2} \sqrt{\left(\frac{l}{L}\right)^2 + \left(\frac{m}{W}\right)^2 + \left(\frac{n}{H}\right)^2} \quad (3)$$

in which, l, m, n are mode indices indicating the x -, y -, and z -directions respectively. L, W , and H indicate the respective length, width and height of the plenum. The modes involving a single dimension are termed axial modes. For example, this would include the $(1, 0, 0)$ and $(0, 2, 0)$ modes. Tangential modes involve two dimensions (i.e. the $(1, 0, 1)$ and $(0, 2, 1)$ modes). Oblique modes involve three dimensions (i.e. the $(1, 1, 1)$ or $(2, 1, 2)$ modes). The error between measured and predicted natural frequencies is less than 5 Hz.

4. Results and discussion

Fig. 6 demonstrates the attenuation due to introducing an MPP absorber. In this plot, a type of insertion loss is shown. The differ-

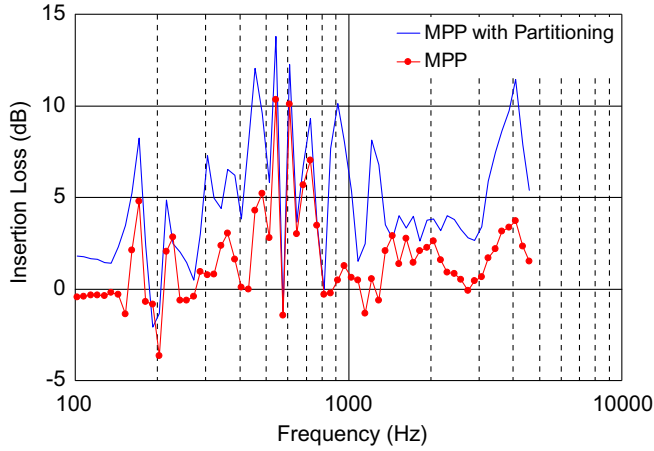


Fig. 6. Insertion loss comparison in 1/12 Octave bands.

ence was determined between a spatial average of the mean square sound pressure (from 54 sound pressure measurements) on a plane 30 mm anterior to the MPP absorber and a baseline case with no MPP absorber treatment. This insertion loss is shown in 1/12 Octave bands. The figure also includes a curve showing the effect of partitioning added posterior to the MPP absorber. As anticipated, introducing partitioning improves the effectiveness of the treatment. The overall insertion loss of the MPP absorber without posterior partitioning is 1.5 dB while adding partitioning improves the performance by 3.2 dB. Overall insertion loss is calculated by determining the overall spatially averaged mean square sound pressure on the measurement plane for the treated and untreated cases and taking the difference. Notice the distinct lower frequency peaks due to the acoustic modes in the plenum. At higher frequencies, the response is quasi diffuse in nature, and the attenuation of the MPP absorber is less irregular.

Fig. 7 shows the narrowband insertion loss from 0 to 1000 Hz, and also notes the acoustic modes which correspond to some of the more prominent insertion loss peaks. Observe that the insertion loss peaks and nadirs occur at acoustic resonances and anti-resonances respectively.

This information is summarized in Table 1. Table 1 shows the insertion loss at different modal frequencies for the MPP with and without partitioning. The table separates the modes by their

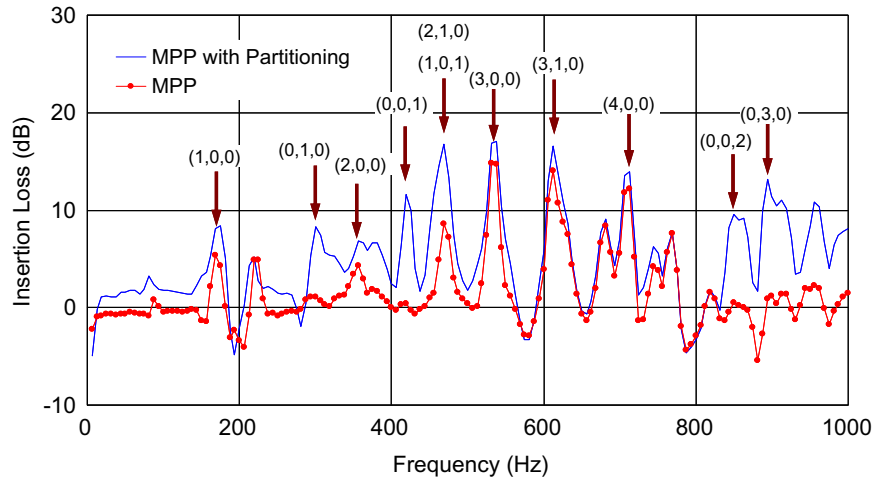


Fig. 7. Insertion loss below 1000 Hz including corresponding modes in narrow bands.

Table 1
Insertion loss at modal frequencies for MPP with and without partitioning.

	x	y	z	Frequency (Hz)	MPP insertion loss (dB)	MPP with partitioning insertion loss (dB)	MPP insertion loss (averaged) (dB)	MPP with partitioning insertion loss (averaged)
Axial modes in x-direction	1	0	0	178	5.4	8.1	11.2	13.3 dB (improve 2.2 dB)
	2	0	0	357	4.3	6.8		
	3	0	0	535	14.7	17.0		
	4	0	0	713	12.2	13.9		
Axial modes in y and z	0	1	0	301	0.7	7.5	0.6	8.8 dB (improve 8.1 dB)
	0	0	1	418	0.4	11.6		
	(0, 2, 0), (0, 0, 2), etc. total six modes							
Tangential modes in y and z	0	1	1	515	0.1	4.5		
	0	1	2	889	-2.7	9.9		
	(0, 2, 1), (0, 3, 1), etc. total six modes							
Tangential modes involves x	1	1	0	350	3.4	5.3	4.3	8.8 dB (improve 4.4 dB)
	1	0	1	455	1.5	11.7		
	(2, 1, 0), (2, 0, 1), etc. total 19 modes							
Oblique modes involves x, y and z	1	1	1	545	6.2	10.3		
	2	1	1	627	6.3	10.9		
	(3, 1, 1), (1, 2, 1), etc. total 19 modes							

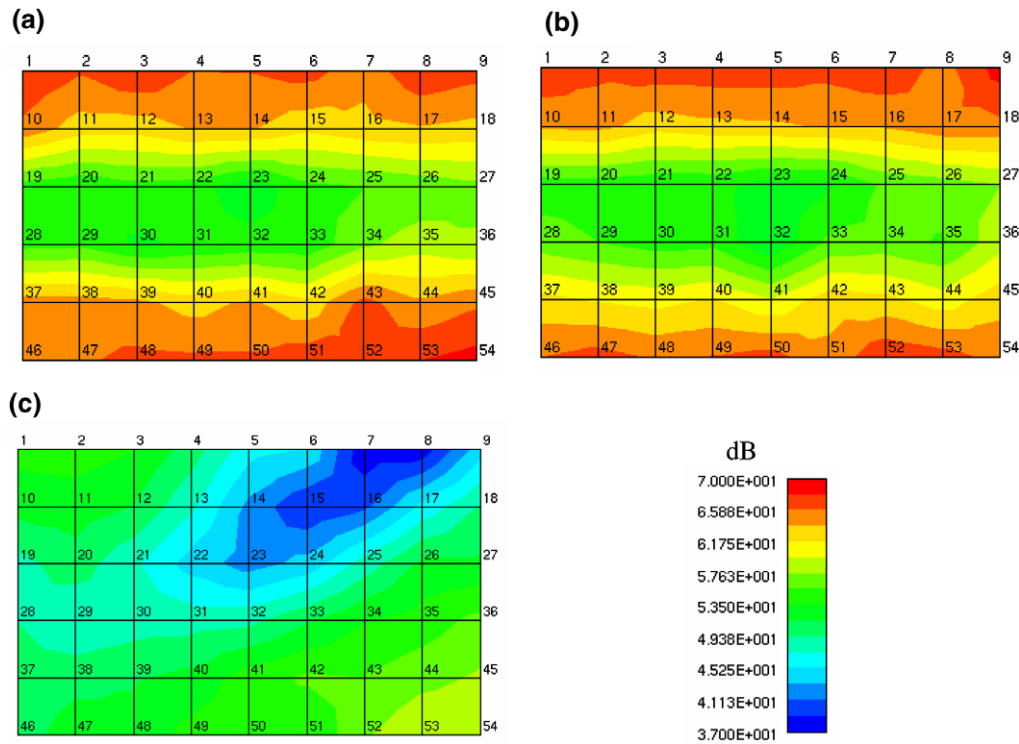


Fig. 8. Measured sound pressure contour map at 418 Hz, corresponding to z -axial mode (0, 0, 1). (a) Untreated, (b) with MPP absorber, (c) MPP absorber with partitioning.

different behavior (i.e. axial, tangential or oblique). Notice that the MPP is effective without partitioning for axial modes in the x -direction (11.2 dB average insertion loss). This corresponds to the effect noticed by Fenech et al. [14]. This can be likened to a normal incident wave being absorbed. In contrast, axial modes in the y - and z -directions have an average insertion loss of less than 1 dB without partitioning posterior to the MPP. Notice that partitioning improves the attenuation by over 8 dB for axial modes in the y - and z -directions. However, the effect is modest for modes in the x -direction (2.2 dB). The results suggest that the partitioning disrupts the mode shape in the neighborhood of the MPP. This will be illustrated via contour maps in the subsequent section.

The tangential and oblique modes further support this mode disruption premise. Notice that the insertion loss improves by over 8 dB for tangential modes that do not involve the x -direction. However, the insertion loss gains are more modest for tangential and oblique modes involving the x -direction (4.4 dB improvement).

Fig. 8 shows a measured sound pressure contour map (for a plane 30 mm anterior to the MPP absorber) at a frequency corresponding to the (0, 0, 1) mode in the z -direction. Contour maps are shown for the aforementioned three conditions (untreated, MPP absorber, MPP absorber with partitioning). Notice that the contour maps are essentially identical for the first two conditions. However, introducing partitioning reduces the sound pressure while also disrupting the acoustic mode.

5. BEM simulation of the MPP with air cavity partitioning

Since the measurement was made on single plane, a BEM simulation was conducted in order to better understand the modal behavior inside of the duct. Simulations were conducted for the three cases mentioned earlier. The indirect BEM [18] was used for each simulation. The MPP itself was modeled via a transfer impedance relationship. The transfer impedance (Z_{tr}) [16] can be written as

$$Z_{tr} = \frac{p_1 - p_2}{u} \quad (4)$$

where p_1 and p_2 are the sound pressures anterior and posterior to the MPP respectively and u is the particle velocity (see Fig. 1). This transfer impedance was defined on the boundary elements representing the MPP.

The BEM mesh with MPP and partitioning is shown in Fig. 9. The mesh consisted of 6532 nodes and 4845 elements. The partitioning was modeled as being square in cross-section instead of hexagonal due to ease of discretization. The cells were approximately 5.25 cm in length and height which was less than the acoustic wavelength

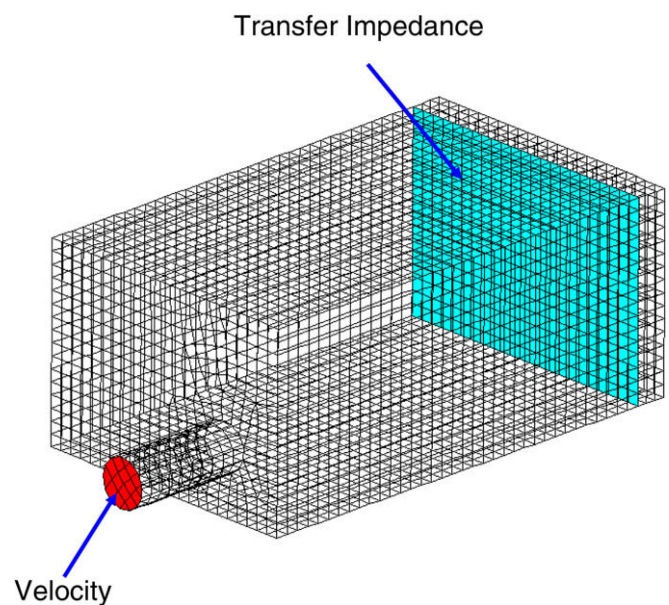


Fig. 9. BEM mesh of plenum with MPP and partitioning.

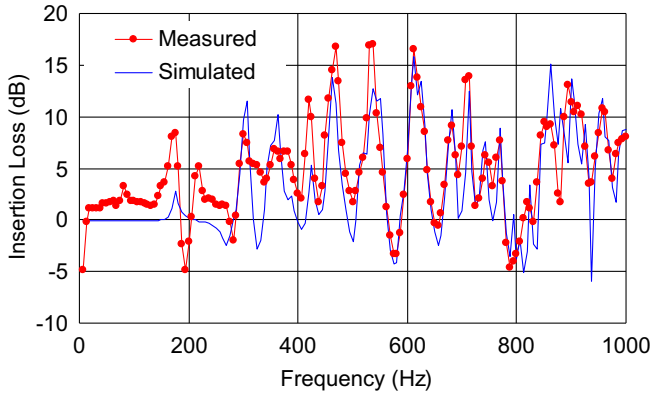


Fig. 10. Insertion loss comparison of MPP with partitioning.

for the maximum frequency of interest (34.3 cm). It was assumed that the MPP and the sides of the plenum were rigid. Though the partitioning was cardboard (and not rigid) in the experiment, the partitioning was assumed to be rigid in the BEM model in order to simplify the modeling. A velocity of 1 m/s was assumed at the inlet as shown in Fig. 9. Linearity is assumed. Thus, the sound pressure and particle velocity results should be correct in the phenomenological sense but the levels will be high.

A small amount of absorption was added to the plenum cavity for each of the cases by using a complex speed of sound with a small imaginary component as described in Ref. [19]. This absorption added to the cavity partially accounts for the absorption intro-

duced due to the vibration and absorption of the plenum surface and the cardboard backing.

Fig. 10 shows insertion loss for the MPP with partitioning. The measured results are compared to BEM simulation. Notice the good agreement in the results between 300 and 1000 Hz. In particular, the BEM simulation correctly predicts most of the peaks and nadirs in the insertion loss. Below 300 Hz, the simulation did not compare well. This might partially be due to background noise since a bookshelf loudspeaker was used and it produces little sound power at low frequencies. Furthermore, the measurement results are questionable at low frequencies because it is not expected that the MPP would provide much attenuation below the first mode of the plenum since the measured absorption (shown in Fig. 5) was quite low. It is also possible that the cardboard partitioning provides a small amount of absorption at low frequencies. Nevertheless, the good agreement above 300 Hz suggests that the model is realistic.

Notice the negative insertion loss in both the measurement and simulation at several frequencies. This is because the MPP adds damping to the cavity at both the resonances and anti-resonances. At the anti-resonances, this manifests itself as a negative insertion loss. In both simulation and the measurement, plenum resonant frequencies shifted little. The MPP and adjoining cavity may have little effect because the cavity depth (6.5 cm) is small compared to the dimensions of the plenum.

Fig. 11 shows BEM sound pressure contour plots inside of the plenum. Several field point planes were constructed along the length of the plenum as indicated in the figure. Results are shown for the (0, 1, 0) mode. Fig. 11a and b shows the contour plots for the untreated and MPP unpartitioned cases.

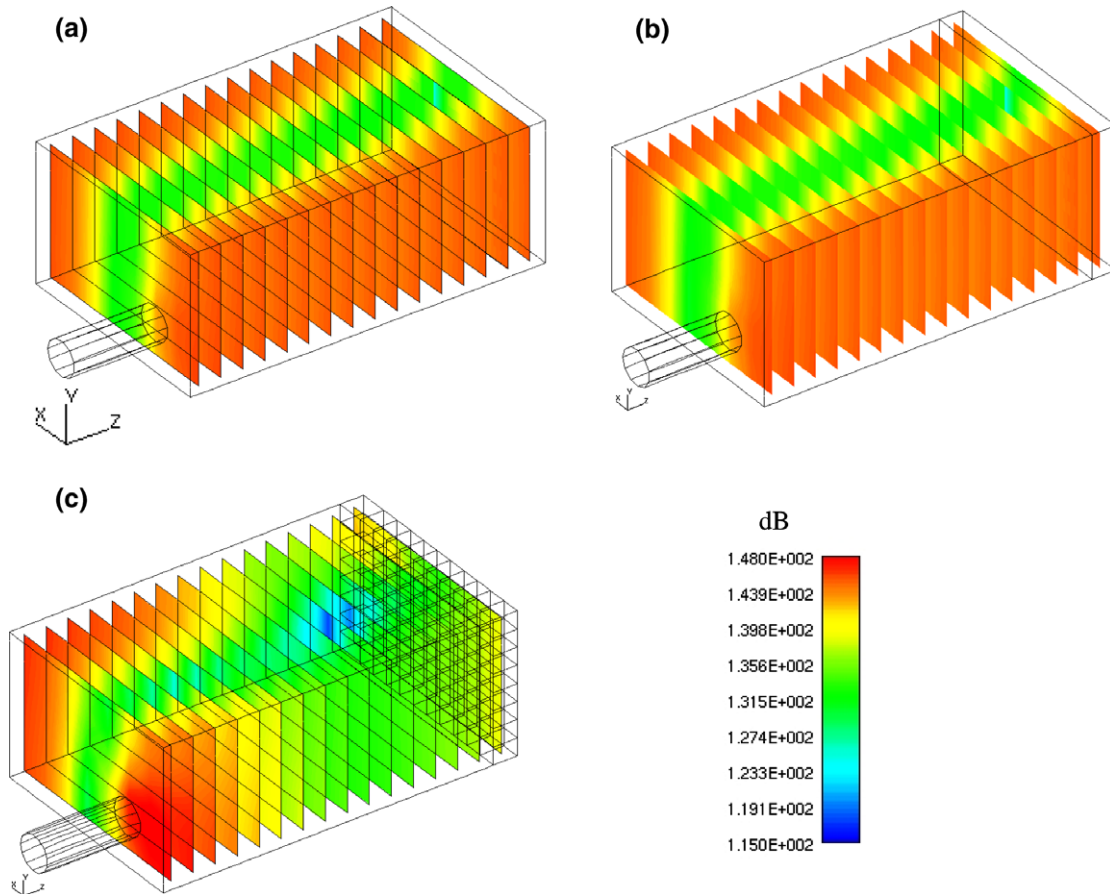


Fig. 11. Simulated sound pressure contour map at 294 Hz, corresponding to y-axis mode (0, 1, 0). (a) Untreated, (b) with MPP absorber, (c) MPP absorber with partitioning.

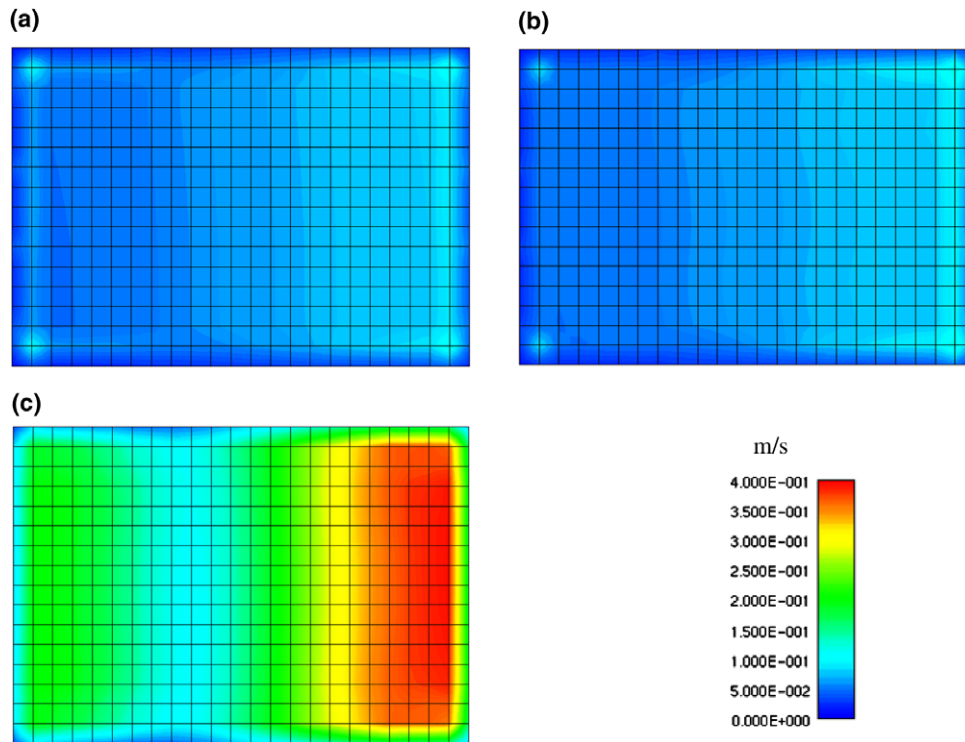


Fig. 12. BEM simulated particle velocity (normal to the MPP) contour map at 294 Hz, corresponding to y -axial mode (0, 1, 0). (a) Untreated, (b) with MPP absorber, (c) MPP absorber with partitioning.

Fig. 11c shows the sound pressure contour for the MPP with partitioning. Notice that the sound pressure is low close to the MPP but the (0,1,0) mode is still present close to the source (further from the MPP).

Fig. 12 shows particle velocity (normal to the MPP) on a plane 25 cm anterior to the MPP. Note that particle velocity is not shown right on the BEM mesh since field point results for particle velocity are inaccurate when located on the BEM mesh itself. Nevertheless, 2.5 cm is much less than an acoustic wavelength at 295 Hz so the results shown should approximate the particle velocity at the MPP. Notice that the unpartitioned MPP (Fig. 12b) has very little effect because the particle velocity in the direction normal to the MPP panel is quite low (nearly the same as for the untreated case shown in Fig. 12a). This suggests that the pressure difference between sides of the panel is low. The partitioning insures that the (0,1,0) mode behavior will not manifest itself behind the MPP. This leads to a higher particle velocity in the perforate (Fig. 12c) resulting in greater energy dissipation or damping in the perforate.

6. Conclusions

The effect of adding a partition in the back cavity of an MPP absorber has been investigated. The results indicate that partitioning improves the performance of the absorber by disrupting wave propagation behind the MPP that would be present without it. The effect is particularly noticeable at low frequencies where the acoustic response is resonant in nature. In that case, partitioning improved the MPP performance by over 8 dB for the example included in this paper. However, attenuation gains are more modest if the modes propagate perpendicular or oblique to the MPP absorber (less than 5 dB). Contour maps at a few frequencies of interest confirmed the hypothesis.

Additionally, a BEM analysis was conducted to simulate the effect of the MPP plus air cavity. Analyses were conducted with and

without partitioning in the adjoining cavity. The simulation agreed well with experimental results when it was assumed that the MPP could be modeled via a transfer impedance boundary condition. The simulation illustrated that the MPP was most effective when the particle velocity (in the direction normal to the MPP) in the perforations was high.

It is suggested that further MPP work could be focused on HVAC and muffler applications. The impact of partitioning could also be evaluated for engine enclosures, aircraft fuselages and building interiors.

Acknowledgment

The authors are grateful for the support of the Vibro-Acoustics Consortium.

References

- [1] Wu MQ. Micro-perforated panels for duct silencing. *Noise Control Eng J* 1997;45(2):69–77.
- [2] Fuchs HV, Zha X. Acylic-glass sound absorbers in the plenum of the Deutscher Bundestag. *Appl Acoust* 1997;51(2):211–7.
- [3] Maa DY. Theory and design of Microperforated-panel sound-absorbing construction. *Sci Sin* 1975;XVIII:55–71.
- [4] Maa DY. Microperforated-panel wideband absorbers. *Noise Control Eng J* 1997;29(3):77–84.
- [5] Maa DY. Potential of microperforated panel absorber. *J Acoust Soc Am* 1998;104(5):2861–6.
- [6] Liu J, Herrin DW, Seybert AF. Application of micro-perforated panels to attenuate noise in a Duct. *SAE 2007 transactions journal of passenger cars: mechanical systems* 2007-01-2196; 2007. p. 1629–33.
- [7] Fuchs HV, Zha X. Sound-absorbing glass building component or transparent synthetic glass building component. US patent 5700527; 1997
- [8] Chen Y, Liu Y. Microperforated panel silencer for duct elbow. Chinese Patent 2001:2451862.
- [9] Yairi M, Sakagami K, Morimoto M, Minemura A. Acoustical properties of microperforated panel absorbers with various configurations of the back cavity. In: *Proceeding of ICSV12, Lisbon, Portugal; 2005.*
- [10] Sum KS, Pan J, Peng SZ. In: Use of parallel Microperforated panel subabsorbers for noise control in ducts. In: *Proceeding of ICSV13, Vienna: Austria; 2006.*

- [11] Zhang ZM, Gu XT. The theoretical and application study on a double layer Microperforated sound absorption structure. *J Sound Vib* 1998;215(3): 399–405.
- [12] Toyoda M, Takahashi D. Sound transmission through a microperforated-panel structure with subdivided air cavities. *J Acoust Soc Am* 2008;124(6): 3594–603.
- [13] Hillereau N, Syed AA, Gutmark EJ. Measurements of the acoustic attenuation by single layer acoustic liners constructed with simulated porous honeycomb cores. *J Sound Vib* 2005;286(1–2):21–36.
- [14] Fenech B, Keith G, Jacobsen F. The use of microperforated plates to attenuate cavity resonances. *J Acoust Soc Am* 2006;120(4):1851–8.
- [15] Maa DY. Theory of microslit absorbers. *Acta Acust Peking* 2000;25(6):481–5 [in Chinese].
- [16] Wu TW, Cheng CYR, Tao Z. Boundary element analysis of packed silencers with protective cloth and embedded thin surfaces. *J Sound Vib* 2003;261(1): 1–15.
- [17] ASTM ASTM Standard E1050-98. Standard test method for impedance and absorption of acoustical material using a tube, two microphones and a digital frequency analysis system. Philadelphia: American Society for testing and materials; 1998.
- [18] Vlahopoulos N. Indirect variational boundary element method in acoustics. In: Wu TW, editor. *Boundary element acoustics: fundamentals and computer codes*. Southampton, UK: WIT Press; 2000 [chapter 6].
- [19] Herrin DW, Tao Z, Scalf EL, Allen SA, Seybert AF. Using numerical acoustics to predict the attenuation of HVAC plenums. *ASHRAE Trans* 2007;113(1): 10–8.